Correction

CHEMISTRY, BIOPHYSICS AND COMPUTATIONAL BIOLOGY

Correction for "Effect of cholesterol on the molecular structure and transitions in a clinical-grade lung surfactant extract," by Jenny Marie Andersson, Carl Gray, Marcus Larsson, Tiago Mendes Ferreira, and Emma Sparr, which appeared in issue 18, May 2, 2017, of *Proc Natl Acad Sci USA* (114:E3592–E3601; first published April 17, 2017; 10.1073/pnas.1701239114).

The authors note that Marcus Larsson should be credited for designing the research, contributing new reagents/analytic tools, and writing the paper. The corrected author contributions footnote appears below.

Author contributions: J.M.A., M.L., T.M.F., and E.S. designed research; J.M.A. performed research; C.G., M.L., and T.M.F. contributed new reagents/analytic tools; J.M.A., C.G., T.M.F., and E.S. analyzed data; and J.M.A., C.G., M.L., T.M.F., and E.S. wrote the paper.

www.pnas.org/cgi/doi/10.1073/pnas.1706986114

Effect of cholesterol on the molecular structure and transitions in a clinical-grade lung surfactant extract

Jenny Marie Andersson[a], Carl Grey[b], Marcus Larsson[c], Tiago Mendes Ferreira[d,1], and Emma Sparr[a,1]

[a]Physical Chemistry, Lund University, 221 00 Lund, Sweden; [b]Division of Biotechnology, Lund University, 221 00 Lund, Sweden; [c]Clinical Sciences, Department of Pediatrics, Lund University, S-22185 Lund, Sweden; and [d]NMR Group, Institut für Physik, Martin-Luther-Universität Halle-Wittenberg, 06108 Halle, Germany

Edited by Michael L. Klein, Temple University, Philadelphia, PA, and approved March 22, 2017 (received for review January 24, 2017)

The lipid–protein film covering the interface of the lung alveolar in mammals is vital for proper lung function and its deficiency is related to a range of diseases. Here we present a molecular-level characterization of a clinical-grade porcine lung surfactant extract using a multitechnique approach consisting of ^{1}H–^{13}C solid-state nuclear magnetic spectroscopy, small- and wide-angle X-ray scattering, and mass spectrometry. The detailed characterization presented for reconstituted membranes of a lung extract demonstrates that the molecular structure of lung surfactant strongly depends on the concentration of cholesterol. If cholesterol makes up about 11% of the total dry weight of lung surfactant, the surfactant extract adopts a single liquid-ordered lamellar phase, $L_{\alpha(o)}$, at physiological temperatures. This $L_{\alpha(o)}$ phase gradually changes into a liquid-disordered lamellar phase, $L_{\alpha(d)}$, when the temperature is increased by a few degrees. In the absence of cholesterol the system segregates into one lamellar gel phase and one $L_{\alpha(d)}$ phase. Remarkably, it was possible to measure a large set of order parameter magnitudes $|S_{CH}|$ from the liquid-disordered and -ordered lamellar phases and assign them to specific C–H bonds of the phospholipids in the biological extract with no use of isotopic labeling. These findings with molecular details on lung surfactant mixtures together with the presented NMR methodology may guide further development of pulmonary surfactant pharmaceuticals that better mimic the physiological self-assembly compositions for treatment of pathological states such as respiratory distress syndrome.

lung surfactant | cholesterol | order parameter | solid-state NMR | dipolar recoupling

The air–alveoli interface of human lungs consists of ∼100 m^2 of surface area covered by a 1- to 2-μm-thick film rich in lipids, generally referred to as lung surfactant (LS) (1, 2). The alveolar interfacial film has several important functions, including stabilizing the interface, allowing for area expansions and controlling diffusional transport (3–7). These functions strongly rely on the self-assembly structure, as well as on the mechanical, barrier, and surface properties of the dynamic LS interfacial layer, which in turn depend on its chemical composition and external conditions in terms of compression, hydration, and so on. The main components of LS are phospholipids, cholesterol, and the so-called surfactant proteins representing ∼80, 10, and 10 wt %, respectively (2).

Deficiency of LS in the alveoli, or an imbalance of its chemical composition, induces a number of pathological conditions (8). For instance, neonatal respiratory distress syndrome affects prematurely born infants when LS is not yet matured or is completely lacking; this deficiency may be lethal if left untreated. In these cases, the most common treatment is intratracheal administration of an exogenous LS into the lungs (9). In case of acute respiratory distress syndrome the mortality is 35 to 45% (10) and an effective treatment is clearly lacking (8). An accurate characterization of the molecular structure and dynamics of endogenous and exogenous lung surfactant, together with relating such molecular properties with LS functions, should aid significantly in the development of more efficient treatments. This characterization is also central to pulmonary drug delivery.

The LS lipid–protein mixture forms a thin film at the air–tissue interface, with the proposed structure consisting of a monolayer connected with an underlying multilayer structure (4, 6, 11). The multilayer structure has been proposed to have arrangements similar to the bulk phases formed in LS extracts (LSEs) (6, 12–14) and in clinical multivesicular dispersions (15, 16). Two types of multilayer structures have been observed: lamellar bodies with spherically concentric bilayers and a tetragonal structure called tubular myelin (6, 17).

The macroscopic properties of the LS film naturally depend on the molecular organization and dynamics in the lipid–protein mixture. In particular, surface viscosity, surface tension, compressibility, and transport properties can be altered by changes in phase behavior. Abrupt changes in these properties upon variations in, for example, surface pressure, surface area, temperature, or hydration, can be related to phase segregation and first-order phase transitions, whereas gradual changes can be associated with continuous phase transitions (18). In monolayer model systems composed of dipalmitoylphosphatidylcholine (DPPC), which is the main phospholipid in LS, it has been shown that the addition of small amounts of cholesterol leads to a reduction of the surface viscosity. Furthermore, the surface viscosity of cholesterol-containing monolayers showed a nonlinear response to variations in surface pressure, which was associated with phase changes and domain formation during expansion–compression cycles (19, 20).

Previous characterization of LSE bilayer systems have shown phase segregation with two coexisting bilayer phases with

Significance

Cholesterol is currently removed from most lung surfactant extract preparations used in clinical applications. Cholesterol-depleted samples are also used in most in vitro studies of the lung surfactant layer. In our study we have performed a detailed molecular characterization of the structure of the lung surfactant with regard to cholesterol content and temperature. We show that cholesterol has a strong impact on the phase behavior, structure, and dynamics of the lung surfactant system even at low concentrations. We emphasize the importance of controlling the cholesterol content of the lung surfactant system studied to better mimic the endogenous lung surfactant and develop better preparations for clinical treatments.

Author contributions: J.M.A., T.M.F., and E.S. designed research; J.M.A. performed research; C.G., M.L., and T.M.F. contributed new reagents/analytic tools; J.M.A., C.G., T.M.F., and E.S. analyzed data; and J.M.A., C.G., M.L., T.M.F., and E.S. wrote the paper.

The authors declare no conflict of interest.

This article is a PNAS Direct Submission.

[1]To whom correspondence may be addressed. Email: tiago.ferreira@physik.uni-halle.de or emma.sparr@fkem1.lu.se.

This article contains supporting information online at www.pnas.org/lookup/suppl/doi:10.1073/pnas.1701239114/-/DCSupplemental.

www.pnas.org/cgi/doi/10.1073/pnas.1701239114

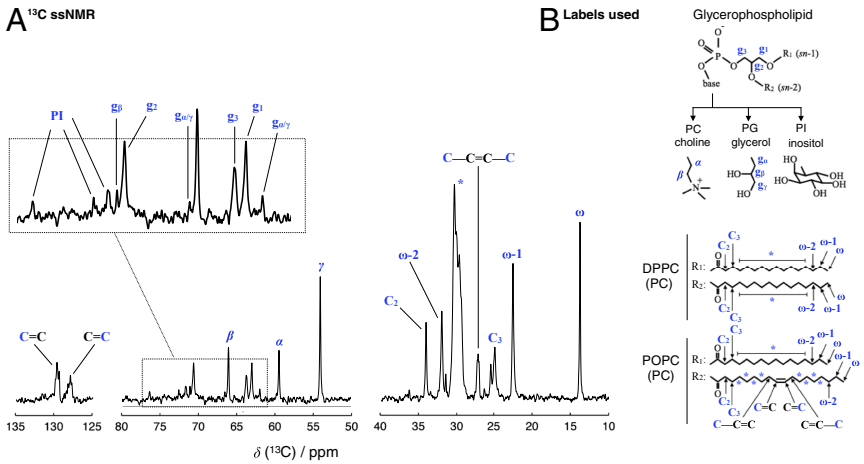

Fig. 1. Chemical analysis of LS components with solid-state NMR. (*A*) A ^{13}C direct polarization solid-state NMR spectrum of clinical-type LSE with peak assignments of phospholipid acyl chains and head groups. (*B*) The labels used to denote distinct phospholipid segments.

different repeat distances (12, 13, 21). The segregated phases have here been assigned as either coexisting lamellar gel and lamellar liquid crystalline (L_α) phases (13) or as coexisting ordered and disordered L_α phases (12). The precise phase behavior strongly depends on the exact composition of the LSE lipid–protein mixture, water content, and solution conditions as well as external conditions such as temperature and pressure. Small variations in any of these parameters may lead to a shift of the positions of the phase boundaries, which may explain the apparent discrepancies between published studies on LSEs obtained at one single temperature.

In the present study we perform a detailed characterization of self-assembly in LS and how this changes with the cholesterol content and temperature. We use a porcine LSE developed for use in clinical treatments and we add or remove cholesterol to this system. Most extracts that are available for clinical use today have reduced cholesterol content [0 to 1 wt % with the exception of Infasurf, which contains 5 wt % cholesterol (14, 22)] compared with the natural LS that contains *ca.* 10 wt % cholesterol (2). LSE samples with low cholesterol content have also been commonly used in biophysical characterization studies (11, 13, 15, 16, 21–24). We aim for an overview picture of the self-assembly in LS mixtures, and we explore phase structure, transitions, and molecular dynamics for a range of cholesterol contents and temperatures. The LS film at the alveolar interface is highly dynamic and exposed to cyclic perturbations during breathing, which may induce inhomogeneities in terms of composition and phase behavior. We are therefore motivated to go beyond the characterization of complex mixtures at fixed conditions and explore what the accessible self-assembly states are by varying intensive variables in the system, for example temperature or pressure. We demonstrate that the addition of physiological amounts of cholesterol has a strong effect on the LS self-assembled structures and molecular dynamics, and we argue that LSE–cholesterol mixtures may better mimic the structure of endogenous LS than the commonly used clinical LSEs with very low cholesterol content. The LSE is compared with simple model systems composed of phospholipids and cholesterol, showing clear similarities as well as distinct differences in terms of self-assembled structures and phase transitions.

We apply solid-state nuclear magnetic resonance (ssNMR) spectroscopy together with small- and wide-angle X-ray scattering (SAXS/WAXS) and MS to characterize reconstructed membranes of the LSE. The same extract has previously been shown to form multilayers at the air–water interface (11). The ssNMR experiments performed, R-type proton detected local field (R-PDLF) 2D spectroscopy (25), ^{13}C direct polarization (DP), ^{1}H–^{13}C cross-polarization (CP) (26), and ^{1}H–^{13}C refocused insensitive nuclei enhanced polarization transfer (rINEPT) (27, 28), were all done using samples of LSE with natural abundance of isotopes and without any insertion of probe molecules.

The experimental characterization of LSE presented provides detailed molecular information because it enabled measurements of highly resolved site-specific quantitative information from all types of possible coexisting domains in the LSE samples. Namely, it was possible to resolve a large number of segmental order parameters S_{CH} for distinct ^{1}H–^{13}C bonds of different phospholipids in the LSE, which enabled identifying the different phases present in the system and characterizing their molecular structure and dynamics.

Results and Discussion

We have made a detailed characterization, at the molecular scale, of the lipid phases present in samples of porcine LSE with different amounts of cholesterol. The samples are here referred to as clinical-type LSE, a sample representing the extract as developed for clinical use; cholesterol-depleted LSE, which is the clinical-type LSE from which cholesterol has been removed by complexation with β-cyclodextrin; and LSE + 5 wt % cholesterol and LSE + 10 wt % cholesterol, which are prepared by adding cholesterol (5 and 10 wt %, respectively) to the clinical-type LSE. Below we first describe the analysis of the chemical composition, lipid phase behavior, molecular structure and molecular dynamics of the samples and then conclude with a discussion of the biological relevance of our findings. The experiments on the LSE were complemented with studies of simple model mixtures specifically chosen to capture different important aspects of the complex mixtures in terms of phase segregation and domain formation.

Chemical Composition of the Clinical-Type LSE. Because the exact chemical composition of LSEs varies between samples obtained from different extraction protocols (9) we here analyzed the clinical-type HL-10 LSE by means of electrospray MS. The lipid composition agrees well with previous studies of LSEs obtained with similar extraction protocols (5, 17), revealing the presence of several phospholipid classes including phosphatidylcholine (PC), phosphatidylglycerol (PG), phosphatidylethanolamine (PE), phoshatidylinositol (PI), and phoshatidylserine (PS), with DPPC being the major PC molecular component found. The anionic lipid classes (PG and PI) were estimated to 13 wt %

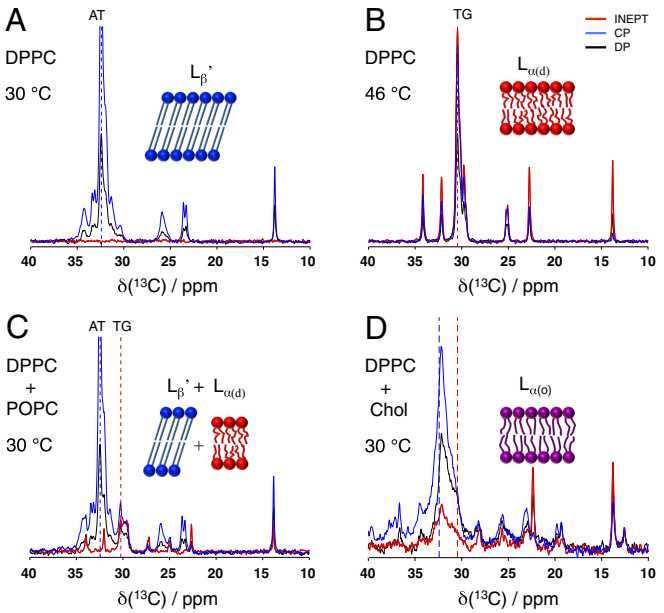

Fig. 2. The ^{13}C DP-CP-rINEPT spectra of different phospholipid phases displaying the chemical shift region of acyl-chain carbons with corresponding illustrations. The maximum intensity of the crowded spectral regions corresponding to acyl chains in an all-*trans* (AT) conformation and *trans/gauche* (TG) conformation is highlighted with blue and red dashed lines, respectively. (*A*) The $L_{\beta'}$ phase of DPPC at 30 °C where the acyl chains are in an AT conformation and from which only CP and DP signals can be recorded. (*B*) The liquid-disordered lamellar phase $L_{\alpha(d)}$ of DPPC at 46 °C where the acyl chains are in TG conformation with the crowded spectral region appearing in both the CP and rINEPT spectra. (*C*) A phase coexistence of $L_{\beta'}$ and $L_{\alpha(d)}$ phases in a DPPC:POPC mixture (76:24 mol %) at 30 °C clearly showing the crowded spectral regions of the distinct phases in the same spectra. (*D*) The liquid-ordered lamellar phase $L_{\alpha(o)}$ of DPPC:chol (65:35 mol %) at 30 °C with the maximum intensity of the crowded spectral region in between the chemical shifts of the AT and TG conformations, recorded in both the CP and rINEPT spectra. At 30 °C the maximum of the crowded spectral region is located near the chemical shift of the AT conformation; however, this position will shift in between the chemical shifts of the AT and TG conformations depending on temperature and cholesterol content.

of the total LSE sample, with PI as the most abundant anionic lipid class, followed by PG. The anionic lipid PS is only present at very low concentrations. For a complete list of all identified lipids and their relative abundance refer to *SI Appendix*, Tables S1–S5. Cholesterol is not detected with the present MS method but was determined by spectrophotometry to be 1.3–1.7 wt %.

The ^{13}C magic angle spinning (MAS) NMR spectroscopy enabled us to resolve a number of carbon peaks from the most abundant lipid species in the LSE, as shown in Fig. 1*A*. The ^{13}C peak assignment was based on previous studies of single lipids species (29, 30). As expected, the ^{13}C NMR spectrum is dominated by signal from the lipid species in the major phospholipid class, PC. The signal originating from saturated lipid acyl chains is mainly located between 10 and 40 ppm, with the crowded spectral region of the lipid acyl chain (asterisk in Fig. 1*A*) with chemical shifts around 29 to 31 ppm. The range in chemical shifts corresponding to the crowded spectral region contains precise information on the conformation of the acyl chains, as will be discussed in more detail below. The signal from unsaturated lipid species, namely from the carbons participating in double bonds and their adjacent methylene groups, also shows high intensities in the spectrum. Peaks from the double bonds in the unsaturated lipids appear at chemical shifts of 125 to 135 ppm, and peaks from the adjacent methylene groups are observed at 27 to 28 ppm.

Peaks originating from phospholipid headgroups are observed at 50 to 80 ppm where PC, PG, and PI headgroups were identified, although PG and PI have rather low intensities (*SI Appendix*, Fig. S1). The chemical shifts of all identified compounds are listed in *SI Appendix*, Table S6. Cholesterol cannot be resolved in the spectra due to low concentration in the clinical-type LSE samples, whereas it is clearly detected in the spectra from LSE samples that were supplemented with cholesterol. We were not able to detect any carbons from amino acids in the LS proteins by MS or NMR, which can be explained by the low protein concentration (2 to 4 wt %) in the LSE sample.

DP-CP-rINEPT Reference Spectra from Model Systems. The CP and rINEPT schemes for ^{1}H–^{13}C polarization transfers are commonly used NMR techniques to enhance the ^{13}C signals in solids and liquids, respectively. However, for the special case of anisotropic liquid crystalline phases that corresponds to the LS lamellar phases investigated, the rINEPT efficiency of a given ^{1}H–^{13}C spin pair depends largely on the time scale of the C–H bond reorientational motion and on its orientation because these two factors determine relaxation rates. For example, the rINEPT becomes inefficient for ^{1}H–^{13}C spin pairs that relax much faster than the 6 ms required for the rINEPT transfer to occur. In such cases, CP transfers may provide better performance over rINEPT because the CP transfer time can be set much shorter (about 1 ms or lower). A more detailed description of the dependence of CP and rINEPT intensities can be found for example, in the publications by Nowacka et al. (31, 32) and Gross et al. (28).

In multilamellar systems, such as the LSE samples studied here, the dynamics and dipolar couplings of the ^{1}H–^{13}C spin pairs will depend on their position in the lipid molecules as well as on the phase of the bilayer. In this context, a combination of CP and rINEPT experiments is most appropriate, because the LSE contains several coexisting lamellar phases with different molecular structural and dynamical features. For instance, the use of CP and rINEPT spectroscopy enables selective detection of the solid- and liquid-like domains, as will be shown below.

To investigate the LSE systems, we first measured DP-CP-rINEPT spectra from the simple and well-characterized model systems DPPC, DPPC/1-palmitoyl-2-oleoyl-*sn*-glycero-3-phosphocholine (POPC), and DPPC/cholesterol, to be used as reference samples. The model systems were chosen to represent the possible lipid phases present in the LSE samples, namely, a lamellar gel phase with solid chains ($L_{\beta'}$) and liquid crystalline lamellar phases with disordered ($L_{\alpha(d)}$) or ordered ($L_{\alpha(o)}$) chains.

In a lamellar gel phase, the acyl chains adopt an all-*trans* (AT) conformation (33) and have reorientation motions with timescales near microseconds (34), the so-called intermediate regime motions in NMR spectroscopy (35). The intermediate-regime motions cause a severe broadening of the ^{13}C NMR peaks as confirmed by the DP-CP-rINEPT spectra of a DPPC lamellar gel phase, $L_{\beta'}$, shown in Fig. 2*A*. Because of the very fast transverse relaxation of ^{1}H and ^{13}C magnetization characteristic of the intermediate-regime motions, the ^{13}C signals from acyl chains are only visible in the CP spectra and not in the rINEPT spectra. Above 42 °C, the DPPC acyl chains melt and a disordered liquid crystalline lamellar phase, $L_{\alpha(d)}$, is formed. Compared with the $L_{\beta'}$ phase, the acyl chains of the $L_{\alpha(d)}$ phase are highly mobile, here meaning much faster than intermediate-regime motions (33). This induces a decrease of the transverse relaxation rates as observed in Fig. 2*B* where the acyl chain peaks are much more narrow and visible in both the CP and rINEPT spectra. The acyl chains in the $L_{\alpha(d)}$ phase become disordered [i.e., adopt *trans/gauche* (TG) conformations], which induces the

shift of the crowded spectral region from 31 to 33.5 ppm in the gel phase to around 29 to 31 ppm in the $L_{\alpha(d)}$ phase. The spectra of DPPC at 46 °C is compared with previously measured spectra of POPC (29) to further ensure the appearance of an $L_{\alpha(d)}$ phase. If DPPC is mixed with POPC, an $L_{\beta'}$ phase and $L_{\alpha(d)}$ phase coexist at temperatures below 42 °C (36). This is observed in Fig. 2*C*, with the crowded spectral region from the $L_{\beta'}$ phase appearing in the CP spectrum at 31 to 34 ppm and the crowded spectral region from the $L_{\alpha(d)}$ phase appearing in both the CP and the rINEPT spectra around 29 to 31 ppm.

When cholesterol is added to DPPC bilayers at concentrations above 25 mol % (corresponding to 15 wt % in the dry lipid sample), a partially ordered liquid crystalline lamellar phase, $L_{\alpha(o)}$, is formed (37–39). In the presence of cholesterol, the phase transition seen in the DPPC/water system at 42 °C is abolished and the $L_{\alpha(o)}$ phase is present over the whole range of temperatures 30 to 46 °C (37). Here, we shall use the definition of the liquid-ordered phase according to Ipsen et al. (37), that $L_{\alpha(o)}$ is a liquid crystalline bilayer phase with higher acyl-chain order, that is, with a much lower population of *gauche* configurations than in an $L_{\alpha(d)}$ phase, and with a greatly reduced membrane-area compressibility. The DP-CP-rINEPT spectra of a DPPC/chol system is shown in Fig. 2*D*. At 30 °C, as cholesterol dissolves in the DPPC bilayer, the acyl chains become partially disordered and have a less dense packing than in the gel phase. Such conformational difference causes the ^{13}C peaks of the crowded spectral region to shift toward the ^{13}C chemical shifts of the liquid disordered phase. Additionally, the faster rotational diffusion of the acyl-chain C−H bonds in a liquid-ordered phase, with correlation times much lower than the microsecond timescale reorientations present in the gel phase, explains the simultaneous appearance of signals in the CP and rINEPT spectra in contrast to the gel-phase from which rINEPT signals are not observed.

Phase Behavior in the Clinical-Type LSE. Fig. 3*B* shows the crowded spectral region of the DP-CP-rINEPT spectra measured from the clinical-type LSE dispersed in an aqueous solution of 150 mM NaCl and 0.2 mM EDTA (50 wt % LSE in the sample) at temperatures within 30 to 46 °C. The spectral features observed for the clinical-type LSE show similarities with the spectra for the simple phospholipid model systems, which are also expected on basis of the high abundance of these phospholipids in the LSE. The LSE spectra in Fig. 3 can therefore be interpreted with Fig. 2 as reference.

At 30 °C, the simultaneous presence of two crowded spectral regions, one at 29 to 31 ppm visible in both the rINEPT and CP spectra, and another at 31 to 33 ppm only visible in the CP spectrum, clearly shows the coexistence of a liquid crystalline lamellar phase and a lamellar gel phase with solid chains. Because it is not possible to determine the tilt angle of the acyl chains from the present experiments, we will use the simplified nomenclature, L_{gel}, when referring to the LSE gel phase. A comparison of the peak at 29 to 31 ppm with the reference spectra measured (e.g., Fig. 2*B*) further indicates that the liquid crystalline lamellar phase detected is disordered ($L_{\alpha(d)}$). In the SAXS curve, the two Bragg peaks from the coexisting lamellar phases partly overlap and it is not possible to resolve the individual repeat distances for the coexisting phases. However, the WAXS spectrum clearly shows a peak at q of 1.5 $Å^{-1}$, which is a signature of solid chains in the lamellar phase (*SI Appendix*, Fig. S2).

As the temperature is raised to 35 °C (Fig. 3*B*) the intensity of the peak around 32 ppm in the CP spectrum decreases, which implies partial melting of L_{gel} phase to an $L_{\alpha(d)}$ phase. This also coincides with the decrease in the CP signal intensity of the peak at 13.8 ppm, originated from the $_{\omega}CH_3$ acyl-chain carbons, and the intensity increase of the rINEPT peaks at 22.7 and 34.3 ppm, corresponding to the $_{(\omega-1)}CH_2$ and the C_2 acyl-chain carbons, respectively (*SI Appendix*, Fig. S3).

At 40 °C (Fig. 3*C*) the crowded spectral region at 31 to 33 ppm in the CP spectrum disappeared completely, which implies complete melting of the L_{gel} phase and formation of an $L_{\alpha(d)}$ phase. This is also supported by the increased intensity of the rINEPT signals at 30, 32.3, and 34.3 ppm and the appearance of the highly resolved peak from the $_{(\omega-2)}CH_2$ segment at 32.3 ppm, which was, at lower temperatures, superimposed with the broad peak of the acyl chains in the L_{gel} phase. At this temperature, one single lamellar phase is observed in the SAXS curve, and the peak at q of 1.5 $Å^{-1}$, is no longer visible in the WAXS spectra (*SI Appendix*, Fig. S2).

Concerning carbon peaks with chemical shifts outside the crowded spectral region, the changes in the DP-CP-rINEPT spectra are not as pronounced. There is only a slight increase of the rINEPT intensity for the peaks originating from carbons in the headgroup (around 50 to 80 ppm). The peaks from methine carbons in the chemical shifts within 125 to 135 ppm have relatively high INEPT signal intensities at 30 °C, and the intensities of these peaks increase only slightly with temperature. This suggests that unsaturated lipids are present in the fluid $L_{\alpha(d)}$ phase at all temperatures investigated. For full spectra refer to *SI Appendix*, Fig. S3.

In summary, the clinical-type LSE system studied changes from coexisting gel and liquid crystalline lamellar phases (L_{gel} + $L_{\alpha(d)}$) to a single fluid lamellar phase ($L_{\alpha(d)}$) in the temperature interval within 30 to 46 °C. We discuss how cholesterol affects this transition in the next section.

Effect of Cholesterol on the Phase Behavior of LSE. Most of the cholesterol that is naturally present in LS is removed in the extraction and purification processes that are performed to obtain the clinical-type LSE (22) and only 1.3 to 1.7 wt % cholesterol remains in the lipid mixture. To investigate accurately the role of cholesterol in the LS mixture, we aimed to remove the remaining cholesterol in the clinical-type LSE using β-cyclodextrin (40). The LSE was analyzed with high-resolution ^1H NMR and TLC before and after the β-cyclodextrin extraction step, showing removal of ∼65% of the cholesterol and no detectable change of the other lipid species in the sample.

The DP-CP-rINEPT spectra from the crowded spectral region of cholesterol-depleted LSE sample are shown in Fig. 3*A*. At 30 °C, the CP intensity of the crowded spectral region at 31 to 33 ppm is clearly enhanced compared with corresponding data for the clinical-type LSE in Fig. 3*B*. This implies that the low amount of cholesterol in the clinical-type LSE is enough to partially destabilize the L_{gel} phase. It is also noted that the spectra from the cholesterol-depleted biological extract closely resemble the spectra obtained for the simple binary system of DPPC:POPC (Fig. 2*C*).

The intensities of the CP peaks from the AT acyl chains decrease with increasing temperature, which can be explained by the partial melting of the L_{gel} phase. Still, for the cholesterol-depleted LSE, the CP peak from the AT chains is still visible even at the highest temperature studied (46 °C). This implies the presence of L_{gel} phase bilayer structures even at temperatures above the melting temperature of the main lipid component, DPPC, which is further confirmed by the presence of a peak in the WAXS spectra of the cholesterol-depleted LSE at 46 °C (*SI Appendix*, Fig. S2). This may be explained by the fact that the LSE sample contains a small fraction of lipid species with longer chains and higher melting temperatures compared with DPPC (*SI Appendix*, Table S1). Furthermore, the water content in the LSE samples is slightly below excess solution conditions, and the melting temperature of the lipid mixture is expected to be higher compared with the fully hydrated system (41–44).

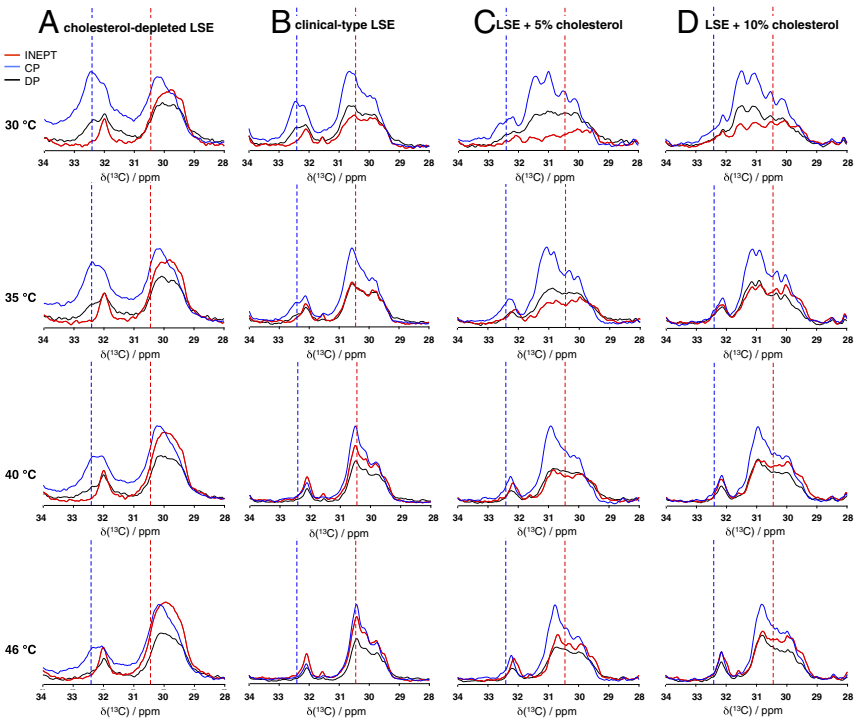

Fig. 3. Zoom-in on the crowded spectral region of the ^{13}C DP-CP-rINEPT spectra of cholesterol-depleted LSE, clinical-type LSE, LSE + 5 wt % cholesterol, and LSE + 10 wt % cholesterol samples. The dashed lines from the reference spectra in Fig. 2 are displayed to aid the interpretation. (*A*) In the spectra of cholesterol-depleted LSE the fraction of the L_{gel} phase is increased compared with the clinical-type LSE and remains present even at 46 °C. (*B*) The spectra from the clinical-type LSE are showing a coexistence of an L_{gel} phase with an $L_{\alpha(d)}$ phase at 30 °C and a gradual melting of the L_{gel} phase with the system adopting a single $L_{\alpha(d)}$ phase at 40 °C. (*C*) In the spectra from the LSE + 5 wt % cholesterol at 30 °C a large fraction of the L_{gel} phase has melted and is coexisting with either an $L_{\alpha(d)}$ and an $L_{\alpha(o)}$ phase or an L_{α} phase with properties in between the $L_{\alpha(d)}$ and $L_{\alpha(o)}$ phases. (*D*) At 40 °C the L_{gel} phase has completely melted and only the L_{α} phase/phases remains. In the LSE + 10 wt % cholesterol a liquid lamellar phase with characteristics of an $L_{\alpha(o)}$ phase is induced at 30 °C. The increase and shift of the crowded spectral region in the rINEPT spectra as the temperature is raised suggests a gradual transition from a phase with characteristics of an $L_{\alpha(o)}$ to one with characteristics of an $L_{\alpha(d)}$ phase. It should be noted that the signal from the $_{\omega-2}CH_2$ group in the rINEPT spectra at 32 ppm belongs to the $L_{\alpha(d)}$ phase and is not part of the L_{gel} or the $L_{\alpha(o)}$ phases.

To further investigate the effect of cholesterol, we added either 5 or 10 wt % of cholesterol to the clinical-type LSE giving total cholesterol content of 6.5 and 11.5 wt %. The results are shown in Fig. 3 *C* and *D*. When 10 wt % cholesterol is added to the LSE sample, there are no signs of an L_{gel} phase at 30 °C. The crowded spectral region with chemical shifts of 30 to 33 ppm is observed in both the CP and rINEPT spectra. The DP-CP-rINEPT spectra resemble the spectrum obtained for the $L_{\alpha(o)}$ phase in the binary DPPC:chol model system (Fig. 2*D*), strongly suggesting that the addition of cholesterol to the biological LSE leads to a conversion of a system with coexisting L_{gel} and $L_{\alpha(d)}$ phases into a single $L_{\alpha(o)}$ phase closely resembling the $L_{\alpha(o)}$ phase in the DPPC:chol model system. The mechanism behind the formation of the $L_{\alpha(o)}$ phase is assumed to be the same as in the model system, which has been described in detail by, for example, Ipsen et al. (37). At higher temperatures, the crowded spectral region of the LSE + 10 wt % cholesterol becomes narrower and shifts to lower chemical shift values, indicating that the amount of acyl chains that are in a *gauche* conformation gradually increases and that the system gradually shifts to an $L_{\alpha(d)}$ phase. Finally, SAXS spectra for both LSE + 10 wt % cholesterol and DPPC:POPC:chol model mixtures show Bragg peaks from lamellar phases with only one repeat distance for the entire temperature interval studied, and no distinct WAXS peaks from phases with solid chains are observed in any conditions (*SI Appendix*, Fig. S4).

For the sample composed of LSE + 5 wt % cholesterol, only a small fraction of the L_{gel} phase remains at 30 °C, and the crowded spectra region from the L_{α} phases closely resembles that of the LSE + 10 wt % cholesterol. As the temperature increases, the crowded spectral region narrows, just as for the LSE + 10 wt % cholesterol sample.

We finally note that peaks from cholesterol are identified in the DP-CP-rINEPT spectra at chemical shifts between 10 and 50 ppm (*SI Appendix*, Fig. S5). These peaks are mainly seen in the CP spectra, because cholesterol has higher C–H dipolar couplings and slower C–H bond reorientations. For full spectra see *SI Appendix*, Figs. S3 and S5–S7.

Molecular Structure in LSE by R-PDLF Spectroscopy. We investigated how cholesterol influences the molecular structure of phospholipid in LSE using R-PDLF NMR spectroscopy (25). This approach is suitable for samples with natural abundance of isotopes. R-PDLF NMR spectroscopy adds an extra dimension to the highly resolved ^{13}C chemical shifts, enabling us to measure for each resolved carbon in the CP and/or rINEPT spectra the magnitudes of its C–H bond order parameters:

$$S_{\mathrm{CH}} = \frac{1}{2}\langle 3\cos^2\theta - 1\rangle, \qquad [1]$$

where θ is the angle between the direction of the C–H bond and the bilayer normal and the angular brackets denote a time average on a timescale of ~10 μs or faster. The S_{CH} magnitudes are determined from the dipolar splittings in a R-PDLF spectra by

$$|S_{\mathrm{CH}}| = \frac{\Delta\nu^{\mathrm{R-PDLF}}}{0.351\, d_{\mathrm{CH}}^{\mathrm{max}}}, \qquad [2]$$

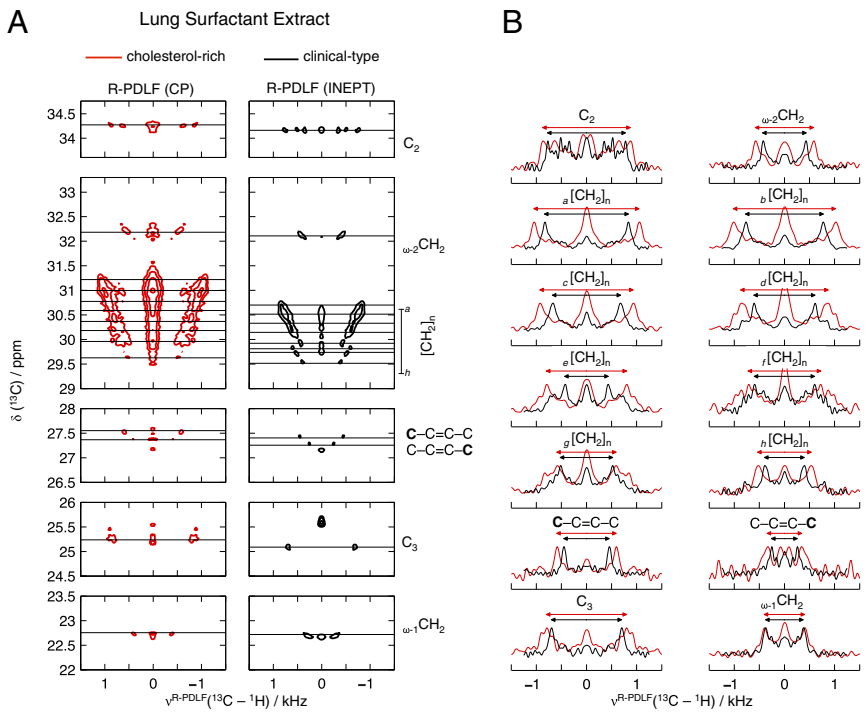

Fig. 4. Selected data from the ^{1}H–^{13}C R-PDLF spectra of the clinical-type LSE (rINEPT as polarization transfer, black lines) and cholesterol-rich LSE (LSE + 10 wt % cholesterol) (CP as polarization transfer, red lines) at 40 °C. (*A*) R-PDLF contour lines at selected spectral regions with lines indicating the chemical shift positions of the R-PDLF dipolar field slices used for determining order parameters. (*B*) The R-PDLF dipolar field slices show clear dipolar splittings $\Delta\nu^{\mathrm{R-PDLF}}$ from different carbons identified in each plot by the dotted lines. The R-PDLF experiments were performed under MAS of 5 kHz, having a total of 32 points in the indirect dimension with increments of 399.6 μs for the clinical-type LSE (the length of two $R18_1^7$ blocks, 18 × 2 × 11.11 μs) and 266.4 μs for the cholesterol-rich sample, each point being acquired under a decoupling strength of 50 kHz, a spectral width of 200 ppm, and with 512 scans. The labels used for the assignment are the same as those given in Fig. 1.

where $d_{\mathrm{CH}^{\max}}$ is the maximum dipolar splitting of a rigid C–H bond and is equal to 22 kHz (45).

Fig. 4 shows selected chemical shift regions of R-PDLF spectra measured from the clinical-type LSE and LSE + 10 wt % cholesterol at 40 °C. A number of splittings $\Delta\nu^{\mathrm{R-PDLF}}$ are remarkably well resolved at many different ^{13}C chemical shifts from which order parameter magnitudes $|S_{\mathrm{CH}}|$ can be calculated. This is a striking result showing that highly quantitative structural information with C–H bond level of detail, that is, $|S_{\mathrm{CH}}|$ values from distinct C–H bonds, can be directly obtained from biological extract of LS without any isotopic labeling.

R-PDLF spectroscopy only enables to measure dipolar splittings from the liquid crystalline lamellar phases. Dipolar slices corresponding to peaks exclusively from the L_{gel} phase, such as the peak at about 32.5 ppm shows extreme broadening and no splitting (*SI Appendix*, Figs. S8–S11). This is because in a phospholipid bilayer with solid chains the occurrence of molecular reorientational motions with correlation times in the microsecond range makes R-PDLF spectroscopy inefficient due to the extremely fast relaxation induced by these motions during the recoupling time.

Unlike solid and gel phases, in L_α phases the reorientation motions of lipids can be separated into two motional regimes, a fast and a slow motion regime, with correlation times much lower and higher than microseconds, respectively, with an absence of reorientations in the intermediate regime of motion (46). The relaxation rates during the dipolar recoupling time are therefore much lower for an L_α phase than for an L_{gel} phase and R-PDLF spectroscopy becomes extremely efficient, yielding highly resolved dipolar splittings as in Fig. 4.

S_{CH} profiles give detailed information on specific lipid segments as well as on the overall phase behavior. Fig. 5 shows $|S_{\mathrm{CH}}|$ profiles derived from the phospholipid acyl-chain splittings in the R-PDLF spectra for the clinical-type LSE, LSE + 5 wt % cholesterol, and LSE + 10 wt % cholesterol. At 30 °C, the $|S_{\mathrm{CH}}|$ values for the fluid fraction of the clinical-type LSE sample were determined to be 0.2 to 0.25 for the first acyl-chain carbons and decrease along the acyl chain and finally reach values close to zero for $_{\omega}CH_3$. The $|S_{\mathrm{CH}}|$ profile closely resembles previously measured S_{CH} profiles of saturated acyl chains in the $L_{\alpha(d)}$ phase (29, 47, 48) in model phospholipid systems with simple composition. The decrease of $|S_{\mathrm{CH}}|$ from the acyl-chain carbons near the glycerol backbone to the carbons at the bilayer center relates to the different probabilities for dihedral rotations along the acyl chains. Because of free volume restrictions, the probability for a *gauche* conformation increases with distance from the bilayer interface and therefore the S_{CH} values decrease toward $_{\omega}CH_3$.

When 10 wt % cholesterol is added to the clinical-type LSE sample there is a strong increase of the maximum value in the $|S_{\mathrm{CH}}|$ profile to above 0.35, which is characteristic of an $L_{\alpha(o)}$ phase (49). Furthermore, the measured $|S_{\mathrm{CH}}|$ values resemble the corresponding values obtained from the $L_{\alpha(o)}$ phase of the binary model system DPPC:chol (38) and the ternary model system of DPPC:DOPC:chol (49). The increase in $|S_{\mathrm{CH}}|$ upon the addition of cholesterol is most pronounced for segments in the crowded spectral region, most likely corresponding to the acyl-chain carbons near C_3. There is also a strong increase for the methylene groups close to the bilayer interface, which was also observed for related model lipid systems (29, 38). The measured $|S_{\mathrm{CH}}|$ profiles for the sample composed of LSE + 5 wt % cholesterol falls in between the measured profiles obtained for the clinical-type LSE and the LSE + 10 wt % cholesterol. This is consistent with a system that contains coexisting $L_{\alpha(d)}$ and $L_{\alpha(o)}$ phases with fast exchange, which implies small-sized domains, or

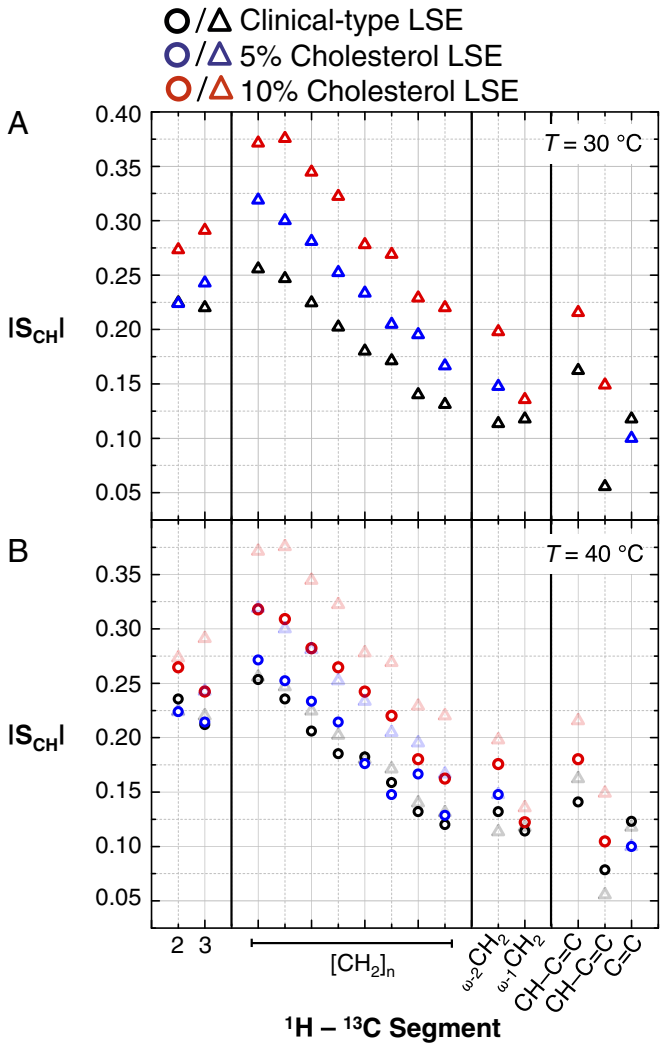

Fig. 5. The $|S_{CH}|$ profiles for the L_α phases of clinical-type LSE, LSE + 5 wt % cholesterol, and LSE + 10 wt % cholesterol. (*A*) At 30 °C, the order parameter profiles of the L_α phase in the clinical-type LSE are characteristic of an $L_{\alpha(d)}$ phase, whereas with the addition of 10 wt % cholesterol the $|S_{CH}|$ profile is closer to that of the $L_{\alpha(o)}$ phase. The $|S_{CH}|$ profile of the LSE + 5 wt % cholesterol indicates either phase coexistence or an L_α phase with properties in between the $L_{\alpha(d)}$ and $L_{\alpha(o)}$ phase. (*B*) $|S_{CH}|$ profiles at 40 °C with the data from 30 °C also plotted with faint triangles. Whereas the $|S_{CH}|$ profile of the clinical-type LSE is insensitive to the temperature change both the $|S_{CH}|$ profiles of the LSE-cholesterol samples approaches that of the clinical-type LSE.

with a single liquid crystalline phase with properties in between the $L_{\alpha(d)}$ and an $L_{\alpha(o)}$ phases. As inferred from the data in Fig. 3*C*, the liquid crystalline lamellar phases coexist with the L_{gel} phase.

Next, we investigated the response in phase behavior when temperature is varied between 30 and 40 °C. As shown in Fig 5*B*, the $|S_{CH}|$ profile for the lipid acyl chains in the clinical-type LSE fluid bilayer does not change significantly in this temperature interval. However, for the LSE + 10 wt % cholesterol sample, the $|S_{CH}|$ values measured at 40 °C are clearly lower compared with the corresponding values measured at 30 °C, approaching the $|S_{CH}|$ profile obtained for the $L_{\alpha(d)}$ phase. This indicates that the liquid crystalline lamellar phase in the LSE + 10 wt % cholesterol gradually changes with increasing temperature, from a phase with the properties typical of an $L_{\alpha(o)}$ phase to a lamellar structure that has properties closer to an $L_{\alpha(d)}$ phase. The observed temperature dependence of the order parameters in the LSE-cholesterol mixtures is in clear contrast to the order parameters of the simple model system composed of DPPC:chol (1:1), which shows an $L_{\alpha(o)}$ phase over this whole temperature range (38, 49). However, there are close similarities between the $|S_{CH}|$ profile of the LSE + 10 wt % cholesterol system and the ternary model system composed of DPPC:DOPC:chol (1:1:1) in the same temperature range (34, 49), with a critical point near physiological temperatures. Based on previous phase diagrams, one can predict that also the DPPC:chol binary system goes through a gradual change from $L_{\alpha(d)}$ to $L_{\alpha(o)}$ at higher temperatures above its critical point (50, 51). The marked change of the $|S_{CH}|$ profile with temperature as observed for both the LSE-chol and DPPC:DOPC:chol systems (34, 49) is likely related to the lowering of the critical temperature where the $L_{\alpha(d)}$–$L_{\alpha(o)}$ coexistence merge into a single L_α phase, due to the presence of unsaturated lipids with low melting temperature. Finally, the $|S_{CH}|$ profile obtained from the LSE + 5 wt % cholesterol approaches the $|S_{CH}|$ profile of the $L_{\alpha(d)}$ phase in the clinical-type LSE at increasing temperature (Fig. 5*B*). The $|S_{CH}|$ profile measured for the cholesterol-depleted sample is similar to that obtained for the clinical-type LSE L_α phase, and again the $|S_{CH}|$ do not change with increasing temperature (*SI Appendix*, Fig. S12).

Biological Relevance. The lipid composition of the LS has a major impact on self-assembly structure, lipid molecular dynamics, domain formation, and phase transitions. These molecular properties are intimately coupled with the macroscopic properties of the LS system. In particular, properties such as surface viscosity, surface tension, compressibility, permeability, and solubility of foreign compounds can be altered by changing the self-assembly structure and molecular dynamics (19, 20, 52). Abrupt changes in these properties upon changes in external conditions or composition can be related to phase segregation and first-order phase transitions, whereas gradual changes can be associated with continuous phase transitions (18). Phase segregation in membranes has been associated with increased permeability and increased solubility of foreign compounds, for example ethanol (53). It may also govern the lateral distribution of membrane-associated proteins, as has been widely explored in relation to so-called lipid rafts in cell membranes (54). Previous studies by Choi et al. (19) and Kim et al. (20) demonstrated nonmonotonic response in surface elastic modulus of phospholipid monolayers with the addition of cholesterol, and the observed effects could be related to domain formation. Similar response of surface properties to changes in phase behavior and domain formation may also occur in the LS layer in the alveoli, where it might have an impact on the structure and function of the LS layer exposed to cyclic perturbations during breathing. For the clinical applications, the lipid phase behavior will also affect formulation properties.

Most clinical formulations used in treatments of neonatal respiratory distress syndrome contain bovine or porcine LS extracted by methanol/chloroform according to the protocol by Bligh and Dyer (55) from bronchoalveolar lavage (BAL) or minced lung tissue. The overall compositions of the lipid extracts of BAL and extracts from minced lungs extracts are similar with only small differences in phospholipid composition (56). The hydrophilic proteins (SP-A and SP-D) are not present in any of the two extract types due to the low solubility in the organic solvents. Furthermore, the extraction of uncharged lipids leads to a reduced cholesterol content in most of these extracts (22), which should be compared with the cholesterol content of 8 to 10 wt % in the endogenous LS (57). In this paper, we demonstrate marked impact of cholesterol content on the structure and dynamics in clinical type LSE, where the high-cholesterol substituted extract is the closest analogy to the in vivo active system in humans and other mammals. Such strong effects on the

phase behavior in the physiological temperature range will most likely also influence the LSE function. Reasonably, the addition of cholesterol to clinical formulations will have an impact on the treatments of LS deficiency-related syndromes (e.g., neonatal respiratory distress syndrome). Several studies have reported negative effects of cholesterol on the performance of LSE (14, 58), even though cholesterol is naturally present in the in vivo LS system. The rationale behind the reported negative effects of cholesterol remains unclear and the discrepancy may be related to differences other than the cholesterol content between the extracts and the in vivo system.

When 10 wt % cholesterol is added to LSE, only L_α phases are formed. By depleting the cholesterol from the system we observe strong phase segregation into an L_{gel} phase with solid chains and an L_α phase with disordered chains at physiological temperatures. It is an important conclusion from the present study that the LSE + 10 wt % cholesterol system forms only L_α phases over the whole range of temperatures between 30 and 46 °C, with the properties of this lamellar system gradually changing with temperature. In other words, the tendency for phase segregation between solid and fluid phases and domain formation is clearly reduced at physiological cholesterol concentrations and at physiological temperatures.

Conclusions

We present a systematic characterization of how cholesterol influences the self-assembly structure in an LSE in great detail and show the effect of different concentrations of cholesterol. In the absence of cholesterol there is a strong segregative behavior and formation of two bilayer phases at 30 °C, an L_{gel} phase and a liquid-disordered lamellar phase $L_{\alpha(d)}$. The transition temperature leading to the formation of a single $L_{\alpha(d)}$ phase takes place close to physiological temperatures. Phase segregation between solid and fluid structures is abolished when the sample is supplemented with physiological levels of cholesterol, and only L_α phases are formed over a relevant temperature interval (30 to 46 °C). The L_α phase has the characteristics of a $L_{\alpha(o)}$ phase at temperatures around 30 °C, which gradually change toward an $L_{\alpha(d)}$ phase when the temperature is increased to 40 °C. This implies a lowering of the critical temperature compared with the minimal system composed of the main LS phospholipid, DPPC, and cholesterol (37). The depression of the continuous $L_{\alpha(o)}$–$L_{\alpha(d)}$ transition can be related to the acyl-chain composition in the lung surfactant, which differs from the model system with only saturated 16:C acyl chains (*SI Appendix*, Tables S1–S5). The structure characteristics of the $L_{\alpha(o)}$ phase closely resemble the cholesterol-rich liquid-ordered domains, similar to so-called lipid rafts in cell plasma membranes. The lipid rafts have been proposed to serve as functional platforms in cell signaling and intercellular membrane trafficking (59, 60). In the LS layer covering the alveolar interface the presence of cholesterol may serve to prevent segregation and domain formation, and the formation of stable fluid bilayer phases, which likely have a strong impact on diffusional transport across the layer as well as mechanical and elastic properties during breathing expansion–retraction cycles (19, 20).

Materials and Methods

Sample Preparation. The LSE used in this study, HL-10, was a kind gift from Leo Pharma, Ballerup, Denmark. The surfactant is extracted from minced porcine lungs by the method of Bligh and Dyer (55). After extraction only the hydrophobic surfactant proteins (SP-B and SP-C) are present in the LSE, at a concentration of 1 to 2% each, with complete removal of the hydrophilic surfactant proteins (56, 61). The 1,2-dipalmitoyl-*sn*-glycero-3-phosphocholine (DPPC), POPC, 1,2-dipalmitoyl-*sn*-glycero-3-phospho-(1′-*rac*-glycerol) (DPPG), and cholesterol were purchased from Avanti Polar Lipids. NaCl, CaCl2, EDTA, β-cyclodextrin, chloroform, and methanol were purchased from Sigma-Aldrich. HL-10 was a clinical-grade pharmaceutical compound assessed for the treatment of adult respiratory distress syndrome (Leo Pharma). It showed promising results in a phase-IIB study but failed to meet primary end points in a phase-III study, and thus was discontinued. The final clinical-grade batches were provided to us and were kept in closed vacuum vials in deep refrigeration until examination. The reason for studying this system is the fact that this material was in a freeze-dried state intended for aqueous resuspension before clinical use. Thus, resuspension in suitable media and further processing becomes a much more controlled process, rather than freeze-drying available clinical-grade natural surfactant material that already is in aqueous dispersion. The LSE was studied in the presence and absence of cholesterol and in different solution conditions. To remove cholesterol, LSE was dispersed in a solution of 20 mM β-cyclodextrin and left for 8 h, and then the aqueous solution was removed by centrifugation. The extract was washed once and then freeze-dried. Model lipid systems were used as reference samples in the study, including DPPC, DPPC:POPC (76:24), DPPC:POPC:cholesterol (50:15:35), and DPPC:cholesterol (65:35). The samples composed of model lipids and samples composed of LSE with added cholesterol were prepared as follows. The lipids were dissolved in chloroform:methanol (2:1) at a concentration of 15 mg/mL. The solvent was then evaporated under a stream of N_2 gas and the samples were left to dry under vacuum overnight. The dried lipid films were then redispersed in 50 wt % aqueous solutions to keep them close to full hydration without having excess water, which would reduce the signal-to-noise ratio from lipids in the ssNMR measurements. The mixtures were heated to 40 °C and vortexed for ∼5 min to ensure proper mixing. The samples were then equilibrated for 48 h at 27 °C before each measurement.

ssNMR. All NMR experiments were done on natural-abundance ^{13}C samples and performed on a Bruker-Avance AVII-500 spectrometer equipped with a Bruker E-free MAS 4-mm probe, at ^{1}H and ^{13}C resonance frequencies of 500 and 125 MHz, respectively. All samples were held in 4-mm inserts and put to a rotor and done under MAS spinning at a frequency of 5,000 Hz (except for spectra in *SI Appendix*, Figs. S10 and S11 acquired at 8 kHz). The inserts were weighed before and after adding the samples to control that the same amount of sample was used in each experiment. The CP (26), DP, and rINEPT (27, 28) experiments all used the same recycle delay, receiver gain, dwell time, number of acquisitions points, and decoupling power. The full setup was as follows: an acquisition time of 96 ms with a recycle delay of 4 s, 512 scans were used for LSE samples and 256 scans for model systems, and the measurements were repeated twice. Radio frequency pulses were set to give the nutation frequencies: 80.65 kHz (^{13}C 90° and 180° pulses), 80.65 kHz (^{1}H INEPT pulses), 50 kHz (^{1}H decoupling pulses), 80 to 100 kHz (^{1}H CP ramp pulse during contact time), and 90 kHz (^{13}C CP pulse during contact time). The rINEPT experiments were made with τ_1 equal to 1.8 ms and τ_2 equal to 1.2 ms. The CP contact time was 1,000 μs. All experiments were recorded with a spectral width of 200 ppm. The R-PDLF experiments (25) were performed by using rINEPT or CP as polarization transfer schemes. Radio frequency pulses were set to give a nutation frequency of 45.0 kHz for the $R18_1^7$ pulses. A total of 16 (*SI Appendix*, Figs. S10 and S11) or 32 (*SI Appendix*, Figs. S8 and S9) steps in the indirect dimension were used with increments 399.6 μs (*SI Appendix*, Fig. S8), 266.4 μs (*SI Appendix*, Fig. S9), or 250 μs (*SI Appendix*, Figs. S10 and S11) and the total number of scans was 512 (*SI Appendix*, Figs. S8 and S9) or 1,024 (*SI Appendix*, Figs. S10 and S11) using a recycle delay of 5 s. rINEPT, DP, and CP experiments were measured at a temperature interval of 30 to 46 °C with steps of 5 °C and R-PDLF experiments were measured at 30 and 40 °C. The chemical shift of the (rINEPT) methyl peak at 13.8 ppm was used as an internal reference. All samples were equilibrated for 30 min before measurements. The temperature was calibrated using methanol (62).

SAXS and WAXS. All SAXS and WAXS measurements were performed on a SAXSLAB Ganesha 300XL with a High Brilliance Microfocus Sealed Tube as X-ray source. Beam shaping is initially done by the shaped multilayer and further collimated by three sets of four-bladed slits. The scattering is detected by a Pilatus detector. The samples were mounted in solid-sample holders (sandwiches) with precut mica windows and heated with a Julabo water bath in the temperature range of 30 to 46 °C. The measurements had a *q*-range of 0.012 to 0.67 $Å^{-1}$ (SAXS) and 0.05 to 2.5 $Å^{-1}$ (WAXS). Data reduction was done with the auto-processing tool of SAXSGUI.

MS. The LSE was dissolved in chloroform:methanol 3:1 (8 mg/mL) with either methylamine (0.2 mM) or ammonium acetate (5 mM) and analyzed using a nano electrospray ionizer connected to an Orbitrap-Velos Pro mass spectrometer (Thermo Scientific). Two-microliter samples were loaded in disposable emitters and sprayed using negative ionization for detection of PE,

PG, PI, and PS lipid species. PC lipid species were identified at both positive and negative ionization (with both methylamine and ammonium acetate). PG, PE, and PI lipid species were quantified using internal standards of each lipid class with hydrocarbon chain lengths 17:0 to 20:4. Data were collected using data-dependent acquisition performing full-scan experiments as well as untargeted MS/MS using higher-energy collisional dissociation fragmentation. The different lipid classes and the acyl-chain composition within each class were identified by their exact mass and characteristic MS^2 fragmentation of the hydrocarbon chains and headgroups as evidence.

Cholesterol Concentration. The cholesterol concentration of the clinical-type LSE was determined by spectrophotometry after oxidation by cholesteroloxidas to 4-cholesten-3-one where hydrogen peroxide is a byproduct. The hydrogen peroxide is reacted with 4-aminophenon and phenol to form a color, which can be measured at 505 and 700 nm. Cholesterol esters are hydrolyzed to free cholesterol by cholesterol esterase. The analysis was performed by the clinical chemistry department at the Lund University Hospital. Cholesterol concentration was further validated by high-resolution ^{1}H NMR based on the integration of the peak from the methyl group of cholesterol and the peak from the methyl group of the choline headgroup (*SI Appendix*, Fig. S13).

ACKNOWLEDGMENTS. We thank Kay Saalwächter for proofreading, Anette Wahlgren and the clinical chemistry department at Lund University Hospital for help with the cholesterol analysis, and Göran Carlström for help with the HR NMR. This work was supported by the Swedish Foundation for Strategic Research (E.S.) and the Swedish Research Council through regular grants and the Linnaeus Center of Excellence "Organizing molecular matter" (to E.S.) and by Deutsche Forschungsgemeinschaft (DFG) through Project ME 4475/1-1 (to T.M.F.). The Knut and Alice Wallenberg Foundation funded the acquisition of the SAXS/WAXS equipment.

1. Hasleton PS (1972) The internal surface area of the adult human lung. *J Anat* 112: 391–400.
2. Casals C, Canadas O (2012) Role of lipid ordered/disordered phase coexistence in pulmonary surfactant function. *Biochim Biophys Acta* 1818:2550–2562.
3. von Neergard K (1929) Neue Auffassungen uber einen Grundbegriff der Atemmechanik. Die Retraktionskraft der Lunge, abhangig von der Ober-flachenspannung in den Alveolen. *Z Gesamte Exp Med* 66:373–394.
4. Goerke J (1974) Lung surfactant. *Biochim Biophys Acta* 344:241–261.
5. Veldhuizen R, Nag K, Orgeig S, Possmayer F (1998) The role of lipids in pulmonary surfactant. *Biochim Biophys Acta* 1408:90–180.
6. Pérez-Gil J (2008) Structure of pulmonary surfactant membranes and films: The role of proteins and lipid-protein interactions. *Biochim Biophys Acta* 1778:1676–1695.
7. Åberg C, Sparr E, Larsson M, Wennerströ H (2010) A theoretical study of diffusional transport over the alveolar surfactant layer. *J R Soc Interface* 7:1403–1410.
8. Zuo Y, Veldhuizen R, Neumann A, Petersen N, Possmayer F (2008) Current perspectives in pulmonary surfactant - inhibition, enhancement and evaluation. *Biochim Biophys Acta* 1778:1947–1977.
9. Roger S, Blanco F (2001) Natural surfactant extract versus synthetic surfactant for neonatal respiratory distress syndrome. *Cochrane Database Syst Rev* 2:CD000144.
10. Bellani G, et al. (2016) Epidemiology, patterns of care, and mortality for patients with acute respiratory distress syndrome in intensive care units in 50 countries. *JAMA* 315:788–800.
11. Follows D, Tiberg F, Thomas R, Larsson M (2007) Multilayers at the surface of solution of exogenous lung surfactant: Direct observation by neutron reflection. *Biochim Biophys Acta* 1768:228–235.
12. de la Serna J, et al. (2013) Compositional and structural characterization of monolayers and bilayers composed of native pulmonary surfactant from wild type mice. *Biochim Biophys Acta* 1828:2450–2459.
13. Gulik A, Tchoreloff P, Proust J (1994) A conformation transition of lung surfactant lipids probably involved in respiration. *Biophys J* 67:1107–1112.
14. Keating E, et al. (2007) Effect of cholesterol on the biophysical and physiological properties of a clinical pulmonary surfactant. *Biophys J* 93:1391–1401.
15. Alonso C, et al. (2004) More than a monolayer: Relating lung surfactant structure and mechanics to composition. *Biophys J* 87:4188–4202.
16. Blanco O, et al. (2012) Interfacial behavior and structural properties of a clinical lung surfactant from porcine source. *Biochim Biophys Acta* 1818:2756–2766.
17. Goerke J (1998) Pulmonary surfactant: Functions and molecular composition. *Biochim Biophys Acta* 1408:79–89.
18. Evans DF, Wennerström H (1999) *The Colloidal Domain: Where Physics, Chemistry, Biology and Technology Meet* (Wiley-VCH, New York), 2nd Ed, pp 493–538.
19. Choi S, et al. (2014) Influence of molecular coherence on surface viscocity. *Langmuir* 30:8829–8838.
20. Kim K, Choi S, Zell Z, Squires T, Zasadzinski J (2013) Effect of cholesterol nanodomains on monolayer morphology and dynamics. *Proc Natl Acad Sci USA* 110:E3054–E3060.
21. Larsson M, Nylander T, Keough KMW, Nag K (2006) An x-ray diffraction study of alterations in bovine lung surfactant bilayer structures induced by albumin. *Chem Phys Lipids* 144:137–145.
22. Larsson M, et al. (2002) Enhanced efficacy of porcine lung surfactant extract by utilization of its aqueous swelling dynamics. *Clin Physiol Funct Imaging* 22:39–48.
23. Larsson M, Larsson K, Nylander T, Wollmer P (2003) The bilayer melting transition in lung surfactant bilayers: The role of cholesterol. *Eur Biophys J* 31:633–636.
24. Bertani P, et al. (2012) Orientation and depth of surfactant protein B C-terminal helix in lung surfactant bilayers. *Biochim Biophys Acta* 1818:1165–1172.
25. Dvinskikh S, Zimmermann H, Maliniak A, Sandström D (2004) Measurement of motionally averaged heteronuclear dipolar couplings in MAS NMR using R-type recoupling. *J Magn Reson* 168:194–201.
26. Pines A, Gibby M, Waugh J (1973) Proton-enhanced NMR of dilute spins in solids. *J Chem Phys* 59:569–590.
27. Morris G, Freeman R (1978) Enhancement of nuclear magnetic resonance signals by polarization transfer. *J Am Chem Soc* 101:760–762.
28. Gross J, et al. (1995) Multidimensional NMR in lipid systems. coherence transfer through *J* couplings under MAS. *J Magn Reson B* 106:187–190.
29. Ferreira T, et al. (2013) Cholesterol and POPC segmental order parameters in lipid membranes: Solid state h-1-c-13 NMR and MD simulation studies. *Phys Chem Chem Phys* 15:1976–1989.
30. Volke F, et al. (1997) Characterisation of antibiotic moenomycin A interaction with phospholipid model membranes. *Chem Phys Lipids* 85:115–123.
31. Nowacka A, Mohr P, Norrman J, Martin R, Topgaard D (2010) Polarization transfer solid-state NMR for studying surfactant phase behavior. *Langmuir* 26:16848–16856.
32. Nowacka A, Bongartz N, Ollila O, Nylander T, Topgaard D (2013) Signal intensities in 1H-13C CP and INEPT MAS NMR of liquid crystals. *J Magn Reson* 230:165–175.
33. Marsh D (1990) *Handbook of Lipid Bilayers* (CRC, Boca Raton, FL), Chap 2.
34. Davis JH, Clair JJ, Juhasz J (2009) Phase equilibria in dopc/dppc-d(62)/cholesterol mixtures. *Biophys J* 96:521–539.
35. Cobo M, Achilles A, Reichert D, de Azevedo E, Saalwächter K (2012) Recoupled separated-local-field experiments and applications to study intermediate-regime molecular motions. *J Magn Reson* 221:85–96.
36. Marsh D (2009) Cholesterol-induced fluid membrane domains: A compendium of lipid-raft ternary phase diagrams. *Biochim Biophys Acta* 1788:2114–2123.
37. Ipsen J, Karlström G, Mouritsen O, Wennerström H, Zuckermann M (1987) Phase-equilibria in the phosphatidyl-cholesterol system. *Biochim Biophys Acta* 905: 162–172.
38. Vist M, Davis J (1990) Phase equilibria of cholesterol dipalmitoylphosphatidylcholine mixtures - ^{2}H nuclear magnetic resonance and differential scanning calorimetry. *Biochemistry* 29:451–464.
39. Thewalt J, Bloom M (1992) Phosphatidylcholine-cholesterol phase diagrams. *Biophys J* 63:1176–1181.
40. Kilsdonk E, et al. (1995) Cellular cholesterol efflux mediated by cyclodextrins. *J Biol Chem* 270:17250–17256.
41. Guldbrand L, Jönsson B, Wennerström H (1982) Hydration forces and phase-equilibria in the dipalmitoyl phosphatidylcholine-water system. *J Colloid Interf Sci* 89:532–541.
42. Ulmius J, Wennerström H, Lindblom B, Arvidson G (1977) Deuteron nuclear magnetic-resonance studies of phase-equilibria in a lecithin-water system. *Biochemistry* 16: 5742–5745.
43. Sparr E, Hallin L, Markova N, Wennerström H (2002) Phospholipid-cholesterol bilayers under osmotic stress. *Biophys J* 83:2015–2025.
44. Smith GS, Sirota E, Safinya CR, Plano RJ, Clark NA (1990) X-ray structural studies of freely suspended ordered hydrated DMPC multimembrane films. *J Chem Phys* 92:4519–4529.
45. Becker J, Comotti A, Simonutti R, Sozzani P, Saalwächter K (2005) Molecular motion of isolated linear alkanes in nanochannels. *J Phys Chem B* 109:23285–23294.
46. Ferreira T, Ollila O, Pigliapochi R, Dabkowska A, Topgaard D (2015) Model-free estimation of the effective correlation time for c-h bond reorientation in amphiphilic bilayers: 1H–13C solid-state NMR and md simulations. *J Chem Phys* 142:044905.
47. Seelig J, Waespesarcevic N (1978) Molecular order in cis and trans unsaturated phospholipid bilayers. *Biochemistry* 17:3310–3315.
48. Perly B, Smith I, Jarrell H (1985) Effects of the replacement of a double bond by a cyclopropane ring in phosphatidylethanolamines - A ^{2}H NMR study of phase transitions and molecular organization. *Biochemistry* 24:1055–1063.
49. Clarke J, Seddon J, Law R (2009) Cholesterol containing model membranes studied by multinuclear solid state NMR spectroscopy. *Soft Matter* 5:369–378.
50. Sankaram M, Thompson T (1991) Cholesterol-induced fluid-phase immiscibility in membranes. *Proc Natl Acad Sci USA* 88:8686–8690.
51. Marsh D (2010) Liquid-ordered phases induced by cholesterol: A compendium of binary phase diagrams. *Biochim Biophys Acta* 1798:688–699.
52. Mouritsen O, Bagatolli L (2005) *Life – As a Matter of Fat: The Emerging Science of Lipidomics* (Springer, Berlin), 2nd Ed.
53. Trandum C, Westh P, Jørgensen K, Mouritsen O (2000) A thermodynamic study of the effects of cholesterol on the interaction between liposomes and ethanol. *Biophys J* 78:2486–2492.
54. Gil T, et al. (1998) Theoretical analysis of protein organization in lipid membranes. *Biochim Biophys Acta* 1376:245–266.
55. Bligh EG, Dyer WJ (1959) A rapid method of total lipid extraction and purification. *Can J Biochem Physiol* 37:911–917.
56. Bernhard W, et al. (2000) Commercial versus native surfactants. *Am J Resp Crit Care* 162:1524–1533.
57. Serrano AG, Pérez-Gil J (2006) Protein-lipid interactions and surface activity in the pulmonary surfactant system. *Chem Phys Lipids* 141:105–118.
58. Zhang H, Wang Y, Neal C, Zuo Y (2012) Differential effects of cholesterol and budesonide on biophysical properties of clinical surfactant. *Pediatr Res* 71:316–323.

59. Rietveld A, Simons K (1998) The differential miscibility of lipids as the basis for the formation of functional membrane rafts. *Biochim Biophys Acta* 1376:467–479.
60. Brown DA, London E (2000) Structure and function of sphingolipid- and cholesterol-rich membrane rafts. *J Biol Chem* 275:17221–17224.
61. Pfizer RH, Soll RF (2005) New synthetic surfactants: The next generation? *Biol Neonate* 87:338–344.
62. Geet ALV (1970) Calibration of methanol nuclear magnetic resonance thermometer at low temperature. *Anal Chem* 42:679–680.